Rainfall downscaling in a space-time multifractal framework

R. Deidda

CRS4, Centro di Ricerca, Sviluppo e Studi Superiori in Sardegna. Cagliari, Italy

Camera-ready Copy for

Water Resources Research

Manuscript-No. ????

Offset requests to:
Roberto Deidda
CRS4
C.P. 94, I-09010 Uta (Cagliari), Italy.

Rainfall downscaling in a space-time multifractal framework

R. Deidda
CRS4, Centro di Ricerca, Sviluppo e Studi Superiori in Sardegna. Cagliari, Italy

Received ?????? – Accepted ??????

Abstract. A space-time multifractal analysis on radar rainfall sequences selected from the Global Atmospheric Research Program (GARP) Atlantic Tropical Experiment (GATE) database is presented. It is shown that space-time rainfall can be considered with a good approximation to be a self-similar multifractal process, so that a multifractal analysis can be carried out assuming Taylor's hypothesis to hold for rainfall over a wide range of spatial and temporal scales. The advection velocity needed to rescale the time dimension is estimated using different tracking techniques. On each selected rainfall sequence, a very good scaling is observed for spatial scales ranging from 4 km to 256 km, and for time scales from 15 minutes to 16 hours. A recently developed scale-covariant multifractal model is then reformulated for numerical simulation of space-time rainfall fields. The two parameters of the log-Poisson distribution used as cascade generator within the model are systematically estimated from each selected rainfall sequence and the dependence of one of these parameters on the large scale rain rate is highlighted. The model is then applied to disaggregate large scale rainfall, and some comparisons between synthetically downscaled and observed rainfall are discussed.

1 Introduction

Multifractal theory [Falconer, 1990; Feder, 1988], initially applied to modeling velocity fluctuations in turbulent flows [Benzi et al., 1984], has been progressively employed, in recent years, also to rainfall modeling. The main reason for the increasing use of the multifractal formalism lies in its capability to achieve, over a wide range of spatial and/or temporal scales, a strong control on the statistical moments of a given distribution of measures, such as turbulent velocity gradients or rainfall data.

Most of the research dealing with multifractal analysis and simulation of rainfall addresses mainly two objectives: 1) "time modeling", i.e., analysis of time series of precipitation and simulation of synthetic series with one-dimensional multifractal models preserving scaling laws observed in real rainfall [Deidda et al., 1999; Georgakakos et al., 1994; Hubert et al., 1993; Ladoy et al., 1993; Menabde et al., 1997; Rodriguez-Iturbe et al., 1989; Svensson et al., 1996], and 2) "space modeling", i.e., analysis and simulation of rainfall distribution in space with two-dimensional multifractal models [Deidda, 1999; Gupta and Waymire, 1993; Kumar and Foufoula-Georgiou, 1993a,b; Lovejoy and Schertzer, 1990; Olson and Niemczynowicz, 1996; Over and Gupta, 1994; Svensson et al., 1996; Tessier et al., 1993]. In the first case, the statistical behavior of rainfall in time is often investigated and eventually simulated without explicit consideration of the spatial distribution and extension of the precipitation field itself. In the second case, the spatial statistical properties of rainfall, accumulated on a fixed time duration, are typically analyzed and simulated without explicitly taking into account the evolution in time of spatial patterns of rainfall. Nevertheless, both these approaches are affected by some limitations, namely they are unable to preserve the covariant properties that characterize real rainfall in both space and time.

For many hydrological applications, a more suitable approach to modeling precipitation fields is needed in order to simulate, in both space and time, the statistical properties observed in real-world precipitation events. For example, the recent profusion of centers for numerical weather forecasting is making rainfall field predictions available for use as input to rainfall-runoff hydrological models for forecasting flood events. In doing so, there is a need to fill the gap in space-time scales between meteorological and hydrological models ("rainfall downscaling"), i.e., to disaggregate the large scale rain-

Correspondence to: Roberto Deidda

fall forecasts to the smaller response scales of hydrological catchment models. This paper tries to bridge the gap between meteorological and hydrological model scales by developing a simple multifractal downscaling framework that preserves space-time statistical properties observed in real rainfall.

With regards to the problem of space-time analysis and simulation of rainfall, we need to make the time variable dimensionally equivalent to space variables. This equivalence can be pursued by rescaling the time dimension by a velocity parameter U, so that rainfall can be regarded as a three-dimensional process in a Eulerian coordinate system frozen in time, where two coordinates are for space and the third coordinate is the rescaled time (Ut). In a multifractal framework one can essentially distinguish two kinds of assumptions on the scaling behavior of rainfall: the first one is that space-time rainfall displays self-similarity, while the second one regards space-time rainfall as being a self-affine process. The choice between a self-similar or self-affine multifractal framework has important implications for the behavior of the rescaling velocity parameter.

The self-similarity assumption corresponds to the Taylor hypothesis of "frozen turbulence" [Taylor, 1938] that has been widely applied in turbulence to characterize velocity fluctuations in space from time series of velocity measurements taken at a fixed point; in other words, the Taylor hypothesis reinterprets the temporal variations at a fixed location as being spatial variations. In a similar way we can introduce the Taylor hypothesis to characterize the space-time statistical properties of rainfall as being a three-dimensional homogeneous and isotropic process where a measure on a scale λ along the (rescaled) time axis is the trace of rainfall on a time $\tau = \lambda/U$, but at fixed location. If self-similarity holds for space-time rainfall the process is forced by a large-scale advection velocity that is constant at any scale λ.

The second assumption is a generalization of the Taylor hypothesis for self-affine processes, where a scale-dependent velocity parameter $U_\lambda \sim \lambda^H$ is used to rescale the time variables. This kind of scaling is expected for passive scalar fields that are advected by atmospheric turbulence with an exponent $H \approx 1/3$. Tessier et al. [1993] have proposed a theoretical framework for space-time transformations of rainfall to interpret the anisotropy related to self-affinity using generalized scale invariance [Lovejoy and Schertzer, 1985; Schertzer and Lovejoy, 1985]. Assuming this theoretical framework, Marsan et al. [1996] performed some analyses of U.S. composite rainfall datasets derived from NWS radars, but their results have shown $H \approx$ - 0.1 and seem only to display a space-time anisotropy induced by the overall advection. This would imply that the large-scale advection velocity plays a more dominant role in space-time rainfall anisotropy compared to other types of self-affine forcing such as that induced by turbulent velocity fluctuations.

This paper is organized as follows: in section 2 the GATE dataset comprising the radar rainfall scans used for the space-time multifractal analysis is illustrated; in section 3 some evidence for and theoretical aspects regarding the multifractal nature of rainfall in time, in space, and in the space-time domain are reviewed and discussed; in section 4 a self-similar multifractal model for the synthetic generation of space-time rainfall is presented; in section 5 the advection velocity of storms and the scaling anisotropy parameter H are estimated from rainfall sequences selected from the GATE dataset. Section 6 is devoted to space-time multifractal analysis of selected GATE rainfall sequences, while in section 7 the results of simulations of rainfall in the space-time domain are discussed; in section 8 the conclusions of this work are drawn.

2 Data

Statistical properties of rainfall fields are investigated on some sequences of radar scans acquired during the GATE campaign [Hudlow and Patterson, 1979]. Each radar scan is available as 15-min rainfall rate over a 100×100 regular square lattice with a 4-km resolution, but only a 64×64 grid centered on each image was used in this work, since data are really provided only within a 200 km radius from the center of each image. The GATE fields were collected off the eastern Atlantic coast of Africa during two different periods in 1974: the set belonging to the first period from 28 June to 15 July is named GATE1 (1716 frames), while the set belonging to the second period from 28 July to 15 August is referred to as GATE2 (1512 frames). As described in detail in section 5, sequences of consecutive rainfall frames were extracted from the GATE1 and GATE2 datasets (Table 2) in order to perform a systematic multifractal analysis in the space-time domain and to calibrate the two log-Poisson parameters of the scale covariant space-time rainfall model.

3 Some remarks on the multifractal analysis of rainfall

In order to perform a multifractal analysis it is necessary to define the structure functions most appropriate to characterize the statistical properties we are interested in. The choice of structure functions depends on the nature of the field we are analyzing and on the objective of the analysis. While in the study of turbulent flows the structure functions are usually defined through the moments of the velocity gradients at different spatial or temporal scales, in the analysis of rainfall processes it is more advantageous to define structure functions through the moments of integral measures of precipitation. In the downscaling process, for example, we are interested in the links between precipitation amounts over different areas and different accumulation times, since meteorological models supply rainfall forecasts over larger space-time scales than those required by catchment hydrological models.

At the scales involved in the downscaling process, we can introduce an instantaneous rainfall intensity $i(x,y,t)$ continuous in space and time [Fabry, 1996], and then define an integral measure P of rainfall over an area $\lambda_x \times \lambda_y$ and a cumulative time τ as:

$$P_{\lambda_x,\lambda_y,\tau}(x,y,t) = \int_x^{x+\lambda_x} d\xi \int_y^{y+\lambda_y} d\theta \int_t^{t+\tau} d\sigma i(\xi,\theta,\sigma) \quad (1)$$

A downscaling problem can now be formulated as follows: given an amount of rainfall $P_{L,L,T}$ over an area $L \times L$ and a time scale T corresponding to the resolution of a meteorological model, we want to determine the probability distribution of precipitation amounts $P_{\lambda_0,\lambda_0,\tau_0}$ over spatial scales $\lambda_0 \times \lambda_0$ and accumulation times τ_0 that are small enough for catchment modeling. In the following a downscaling process will be referred to using the short formulation $P_{L,L,T} :\rightarrow P_{\lambda_0,\lambda_0,\tau_0}$.

3.1 Time modeling

We can introduce the following structure functions to characterize the statistical properties of rainfall in time, over fixed areas of side λ:

$$S_q(\tau) = \left\langle [P_{\lambda,\lambda,\tau}(x,y,t)]^q_{\lambda=const} \right\rangle \quad (2)$$

where $\langle \cdots \rangle$ is both an ensemble average or an average of samples with different starting times t, and eventually different locations x, y.

The multifractal analysis in time can be performed by investigating the scaling behavior of structure functions (2) for different time scales τ, keeping λ constant. In particular we want to identify one or more ranges of time scales τ where the following scaling law holds:

$$S_q(\tau) \sim \tau^{\zeta_\lambda(q)} \quad (3)$$

Exponents $\zeta_\lambda(q)$ are called multifractal exponents if they are nonlinear functions of the moments q and do not depend on the time scale τ: when these conditions are verified the signal is said to display anomalous scaling laws, i.e. multifractality, in time. Exponents $\zeta_\lambda(q)$ can, however, be strongly dependent on the spatial scale λ and on the type of rainfall event. The dependence on the spatial scale λ of the statistical properties in time was investigated on the GATE datasets and the results of this analysis are summarized in Figure 1 where the multifractal exponents $\zeta_\lambda(q)$ obtained for different areal integrations are compared. The integral measures (1) needed for structure functions (2) were computed avoiding missing data, but including zero precipitation records. A convex shape in the $\zeta - q$ plane is a characteristic feature of multifractal measures, while a straight line identifies a fractal object. The more the convexity is

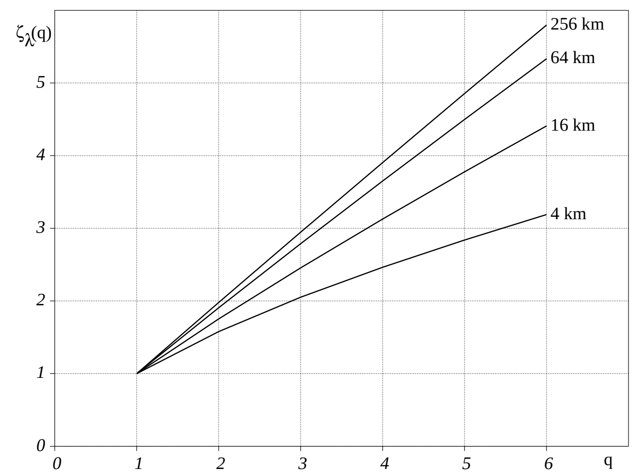

Fig. 1. Multifractal exponents $\zeta_\lambda(q)$ characterizing temporal scaling law (3) of GATE rainfall over square areas having side $\lambda = 4$, 16, 64 and 256 km.

pronounced, the more the measure is intermittent. Figure 1 shows that the more intermittent modes in time are obtained for smaller λ, and thus for smaller areas. This dependence on the spatial scale is highlighted by the subscript λ of exponents $\zeta(q)$ in equation (3). We must also expect that the multifractal behavior of time series from tipping-bucket rain-gauges corresponds to the limit case $\lambda \rightarrow 0$.

Time series of synthetic rainfall over areas of side λ can thus be generated with one-dimensional multifractal models that are able to preserve, for any moment q, the same scaling (3) as estimated on real signals for the corresponding spatial domain.

3.2 Space modeling

If a spatial field of rainfall depths accumulated over a fixed duration τ can be considered as homogeneous and isotropic, the following structure functions can be defined to characterize the spatial multifractal behavior:

$$S_q(\lambda) = \left\langle [P_{\lambda,\lambda,\tau}(x,y,t)]^q_{\tau=const} \right\rangle \quad (4)$$

where $\langle \cdots \rangle$ is an ensemble average or an average of samples with different starting points x, y, and eventually different times t.

The multifractal analysis in space consists then in the search for one or more ranges of spatial scales λ where the following scaling law holds for structure functions (4), keeping the accumulation time τ constant:

$$S_q(\lambda) \sim \lambda^{\zeta_\tau(q)} \quad (5)$$

As for the time analysis, exponents $\zeta_\tau(q)$ are called multifractal exponents if they are nonlinear functions of the moments q and do not depend, in this case, on the spatial scale λ: under these conditions the signal is said to display anomalous scaling laws in space.

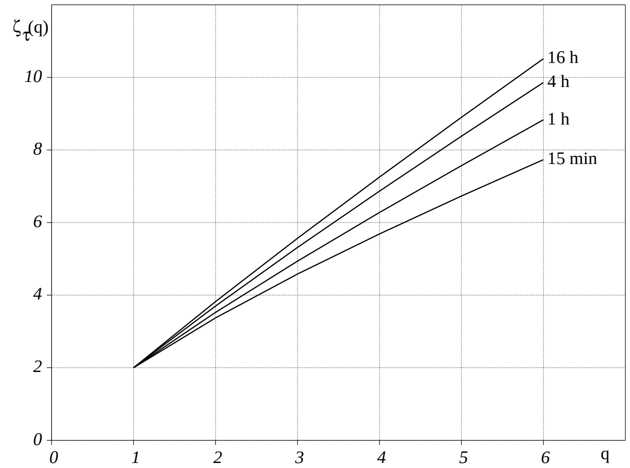

Fig. 2. Multifractal exponents $\zeta_\tau(q)$ characterizing spatial scaling law (5) of GATE rainfall accumulated over times $\tau = 15$ minutes, 1, 4, and 16 hours.

The dependence of the spatial scaling law (5) on the accumulation time τ was recently investigated on the GATE datasets and discussed by Deidda et al. [1999]: rainfall fields are more intermittent in space for shorter accumulation times (Figure 2). This dependence is highlighted by the subscript τ on the exponents $\zeta(q)$ in (5).

Synthetic spatial fields of rainfall depths over a fixed time τ can be generated with two-dimensional multifractal models that are able to reproduce the scaling laws (5).

3.3 Space-time modeling

We now want to formulate the problem of rainfall modeling in a more general way in order to investigate the existence of "universal" scaling laws, characterized by multifractal exponents $\zeta(q)$ that depend neither on the spatial scale λ nor on the time scale τ. The search for these "universal" scaling laws is not the only reason to investigate the "space-time modeling" of rainfall: the solution to the downscaling problem $P_{L,L,T} :\to P_{\lambda_0,\lambda_0,\tau_0}$ suggests this approach as well.

Indeed, one can imagine performing a downscaling process in two steps (Figure 3.a): in the first step rainfall is downscaled in space $P_{L,L,T} :\to P_{\lambda_0,\lambda_0,T}$ with a 2-D model that preserves the scaling laws (5) displaying multifractal exponents $\zeta_T(q)$; in the second step the time downscaling to τ_0 is performed ($P_{\lambda_0,\lambda_0,T} :\to P_{\lambda_0,\lambda_0,\tau_0}$) preserving the scaling (3) with multifractal exponents $\zeta_{\lambda_0}(q)$. Although similar double-step procedures have been already applied to space-time disaggregation of rainfall using, for example, geostatistical techniques [Lebel et al., 1998], the application of this procedure in a multifractal framework can cause, after the second step, the imposed scaling in space to be lost.

In a similar way (see Figure 3.b) one can downscale rainfall first in time $P_{L,L,T} :\to P_{L,L,\tau_0}$ (preserving the scaling (3) with multifractal exponents $\zeta_L(q)$) and then in space $P_{L,L,\tau_0} :\to P_{\lambda_0,\lambda_0,\tau_0}$ (preserving the scaling (5) with multifractal exponents $\zeta_{\tau_0}(q)$), but at the expense of losing the scaling in time.

With a direct "space-time modeling" of rainfall (Figure 3.c) using 3-D multifractal models we can try to reproduce the statistical properties of real rainfall for any intermediate scale λ ($\lambda_0 < \lambda < L$) and τ ($\tau_0 < \tau < T$). Again, after having eliminated the dependence of multifractal exponents on the spatial extension or on the accumulation time, we can better investigate how different kinds of precipitation event or simply the large-scale rain rate can affect the statistical properties.

The problem of space-time modeling is addressed here for both self-similar and self-affine rainfall. In both cases precipitation fields are assumed to be homogeneous and isotropic in space. In the first case, the temporal anisotropy can be eliminated by a rescaling dimensional parameter, i.e. the advection velocity, that is kept constant throughout a wide range of scales; in the second case, a scale-dependent rescaling velocity is used.

Space-time rainfall displaying self-similarity

When the anisotropy between space and time is only related to the overall advection, a simple way to address a space-time analysis and simulation of rainfall is to assume self-similarity and consequently to rescale the time domain with the advection velocity U of the precipitation patterns, thus making the time and space scales equivalent. This approach requires verification that the Taylor hypothesis holds for rainfall fields and that statistical properties along the (rescaled) time dimension are the same as along any spatial dimension. In other words, after having rescaled the time dimension, rainfall fields must be isotropic in each of the three dimensions: two for space, one for time rescaled with U.

If self-similarity holds, we can introduce the following structure functions to characterize the statistical properties in time and space:

$$S_q(\lambda) = \left\langle \left[P_{\lambda,\lambda,\tau=\lambda/U}(x,y,t)\right]^q \right\rangle \tag{6}$$

where $\langle \cdots \rangle$ is both an ensemble average or an average operator over samples with different starting points x, y, t in the space-time domain.

After having estimated the advection velocity U, the multifractal analysis in the space-time domain consists on the search of one or more ranges of spatial scales λ (and the corresponding time scales $\tau = \lambda/U$) where the following scaling law holds for structure functions (6):

$$S_q(\lambda) \sim \lambda^{\zeta(q)} \tag{7}$$

Analogously to the space and time analyses, rainfall can be considered a three-dimensional self-similar multifractal process if at least one range of scales λ is found where the advection velocity U is constant and the scaling law (7) holds with exponents $\zeta(q)$ that are nonlinear

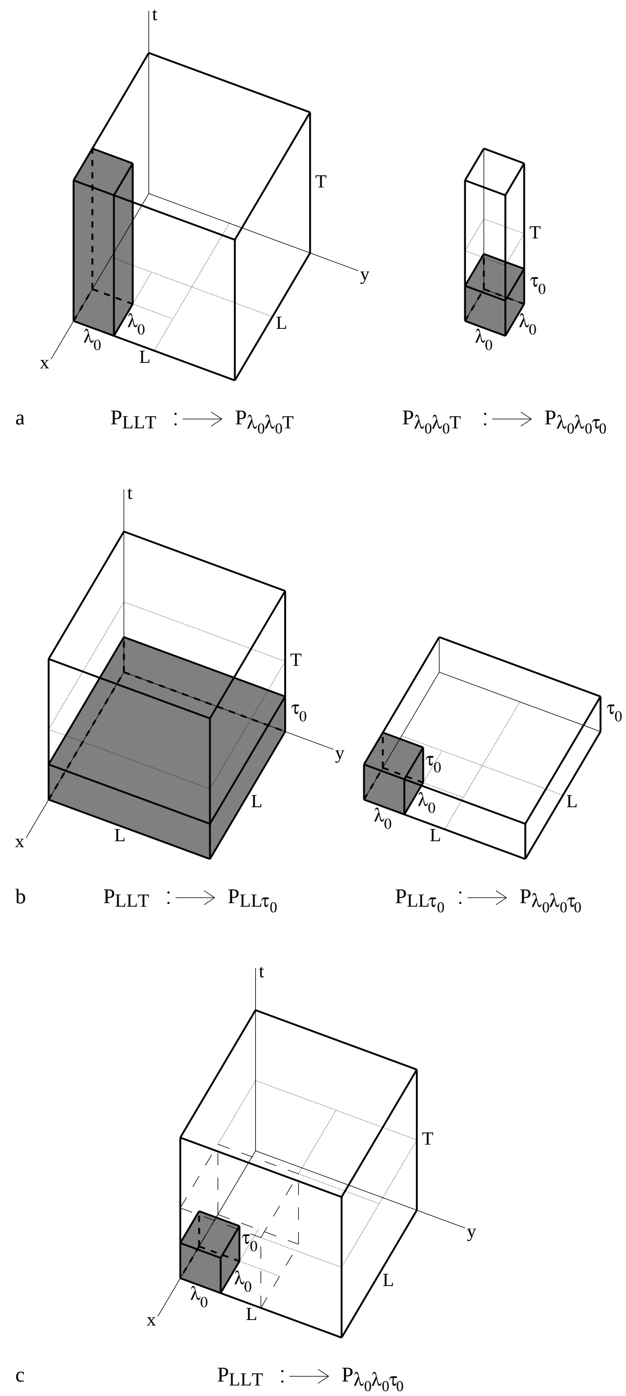

Fig. 3. Different approaches to space-time rainfall downscaling. **a.** Rainfall is first downscaled in space from areas of side L to areas of side λ_0 ($P_{L,L,T} :\rightarrow P_{\lambda_0,\lambda_0,T}$) and then in time from T to τ_0 ($P_{\lambda_0,\lambda_0,T} :\rightarrow P_{\lambda_0,\lambda_0,\tau_0}$). **b.** Rainfall is first downscaled from time T to τ_0 ($P_{L,L,T} :\rightarrow P_{L,L,\tau_0}$) and then in space from scale L to scale λ_0 ($P_{L,L,\tau_0} :\rightarrow P_{\lambda_0,\lambda_0,\tau_0}$) **c.** Direct space-time downscaling ($P_{L,L,T} :\rightarrow P_{\lambda_0,\lambda_0,\tau_0}$).

functions of the moment q and depend on neither the spatial scale λ nor the time scale $\tau = \lambda/U$.

Space-time rainfall displaying self-affinity

A multifractal analysis of space-time rainfall displaying self-affinity can be performed by introducing a scale-dependent velocity parameter $U_\lambda \sim \lambda^H$. Depending on the value taken by the scaling anisotropy exponent H, the following scenarios are possible: i) $H = 0$: the velocity parameter is constant at any scale and the Taylor hypothesis holds; this is the trivial case of self-similarity discussed above; ii) $H > 0$: the scale-dependent velocity parameter U_λ increases with λ; this is the case, for instance, of a passive scalar advected by turbulence, where we must expect $H \approx 1/3$; iii) $H < 0$: velocity increases at smaller scales.

Let us now consider a discrete set of spatial scales $\lambda_n \equiv Lb^{-n}$, where $b \geq 2$ is called the (spatial) branching number. The scale-dependent velocity can be written $U_n \equiv U_{\lambda_n} \equiv U_0 b^{-nH}$. The traveling time needed to advect a quantity along a spatial scale λ_n is thus $\tau_n = \lambda_n/U_n \equiv (L/U_0)b^{-n(1-H)}$, meaning that the discrete set of time scales $\tau_n = Tb_t^{-n}$ to be considered in the space-time multifractal analysis can be obtained by introducing a new (temporal) branching number $b_t = b^{(1-H)}$, which for $H > 0$ or $H < 0$ can be respectively less or greater than the spatial branching number b.

After having estimated both the exponent H and the parameter U_0, we can investigate the existence of one or more scaling regimes (7) for the following structure functions:

$$S_q(\lambda) = \left\langle \left[P_{\lambda,\lambda,\tau=\lambda/U_\lambda}(x,y,t)\right]^q \right\rangle \tag{8}$$

An estimate of the scaling anisotropy exponent H can be obtained by comparing one-dimensional temporal power spectra $E(f_t)$ and one-dimensional spatial spectra, $E(f_x)$ or $E(f_y)$. For a multifractal field we must expect that these spectra follow power-law functions of frequency f_t and wave-numbers f_x or f_y:

$$E(f_t) \sim f_t^{-s_t} \qquad E(f_x) \sim f_x^{-s_x} \qquad E(f_y) \sim f_y^{-s_y} \tag{9}$$

Due to the self-affinity we must also have the following equivalences:

$$\frac{E(b_t f_t)}{E(f_t)} \equiv \frac{E(b f_x)}{E(f_x)} \equiv \frac{E(b f_y)}{E(f_y)} \tag{10}$$

Recalling the relation between the spatial and the temporal branching numbers, equations (9) and (10) yield $b_t^{-s_t} = b^{-s_t(1-H)} \equiv b^{-s_x} \equiv b^{-s_y}$, so that an estimate of the parameter H can be obtained as $H_x = 1 - s_x/s_t$ or $H_y = 1 - s_y/s_t$. If isotropy in space holds, we must find $H_x = H_y = H$.

4 A scale covariant model for space-time rainfall downscaling

A Space-Time RAINfall (STRAIN) model is proposed for hydro-meteorological applications such as rainfall downscaling from the large scales of meteorological models to the scale of interest for rainfall-runoff processes. The model is based on the following assumptions: i) rainfall fields are isotropic and statistically homogeneous in space; ii) self-similarity holds, so that, after having rescaled the time by the advection velocity U, rainfall is a fully homogeneous and isotropic process in the space-time domain (Taylor hypothesis); iii) statistical properties of rainfall are characterized by an "a priori" known multifractal behavior that is determined by the multifractal analysis of observed space-time rainfall. The estimation of the space-time multifractal properties from measured rainfall fields will be addressed later in this paper. The model presented here is a generalization of the multidimensional model by Deidda et al. [1999] for the case of space-time rainfall generation and includes scale covariance by means of an infinitely divisible log-Poisson distribution [Dubrulle, 1994; She and Leveque, 1994; She and Waymire, 1995].

A synthetic space-time rainfall intensity field $i(x,y,t)$ with $(x,y) \in [0,L]^2$ and $t \in [0,T]$, where $T = L/U$, is obtained as a wavelet expansion with coefficients extracted by a stochastic cascade:

$$i(x,y,t) = \sum_{j=0}^{N} \sum_{k_x=0}^{2^j-1} \sum_{k_y=0}^{2^j-1} \sum_{k_t=0}^{2^j-1} \alpha_{j,k_x,k_y,k_t} \psi_{j,k_x,k_y,k_t}(x,y,t) \quad (11)$$

where j is the cascade level index, varying from 0 (first element) to N (number of cascade levels); k_x, k_y and k_t are position indexes on the space-time domain where the signal is generated; $\psi_{j,k_x,k_y,k_t}(x,y,t)$ is a wavelet on level j with position indexes k_x, k_y, k_t; α_{j,k_x,k_y,k_t} is the coefficient extracted from a stochastic cascade.

The three-dimensional wavelets $\psi(x,y,t)$ are defined as a product of three one-dimensional basis wavelets $\Psi(z)$, positive definite and integrable for $z \in [0,L]$ and zero elsewhere:

$$\psi_{j,k_x,k_y,k_t}(x,y,t) = 2^{3j}\Psi(2^j x - k_x L)\Psi(2^j y - k_y L)\Psi(2^j Ut - k_t L) \quad (12)$$

The normalization in the modulus of the basis function $\Psi(z)$ assures the normalization of each wavelet $\psi(x,y,t)$, defined by the above equation. As basis we can use a Gaussian function:

$$\Psi(z) = \begin{cases} c \, \exp\left[-\frac{1}{2}\left(\frac{z-\mu}{\sigma}\right)^2\right] & z \in [0,L] \\ 0 & z \notin [0,L] \end{cases} \quad (13)$$

where $\mu = L/2$, $\sigma = 0.15L$ and $c \cong 1/(\sigma\sqrt{2\pi})$ is a normalization constant.

The random cascade is constructed using a multiplicative process [Monin and Yaglom, 1971, 1975; Yaglom, 1966]; each *son* α_{j,k_x,k_y,k_t} at the j-th level is obtained multiplying the corresponding *father* at level $j-1$ by an independent and identical distributed random variable η, called the generator:

$$\alpha_{j,k_x,k_y,k_t} = \eta \alpha_{j-1,k_x/2,k_y/2,k_t/2} \quad (14)$$

Ensemble averages of q-moments of random variables α can be related to the statistics of the generator:

$$\overline{\alpha^q_{j,k_x,k_y,k_t}} = \overline{\alpha^q_j} = \alpha_0^q \overline{\eta^q}^j \quad (15)$$

Letting $P_{L,L,T} = \int_0^L dx \int_0^L dy \int_0^{L/U} dt i(x,y,t)$ be the integral of the synthetic signal on the domain of generation, the first term of the random process must be:

$$\alpha_0 = \frac{P_{L,L,T}}{\sum_{j=0}^N 2^{3j}\overline{\eta}^j} \quad (16)$$

Structure functions $S_q(\lambda)$ of synthetic precipitation (11) are defined as in equation (6):

$$S_q(\lambda) = \left\langle \left[\int_\xi^{\xi+\lambda} dx \int_\theta^{\theta+\lambda} dy \int_\sigma^{\sigma+\lambda/U} dt \; i(x,y,t) \right]^q \right\rangle \quad (17)$$

where the space-time average $\langle \cdots \rangle$ is computed over all starting points (ξ, θ, σ).

After some computations it can be proved [Deidda et al., 1999] that these structure functions obey the scaling law (7) with expected multifractal exponents $\zeta(q)$ depending only on the ensemble averages of the moments of the generator η:

$$\zeta(q) = q\,(3 + \log_2 \overline{\eta}) - \log_2 \overline{\eta^q} \quad (18)$$

Using the Cauchy-Schwarz inequality it can also be proved that $\zeta(q)$ is a convex and nonlinear function of the moments q, so the model is suitable for generation of multifractal fields. The choice of probability distribution for the random generator η characterizes the multifractal behaviour and the scale covariance of synthetic signals. In this work an infinitely divisible distribution, i.e. the log-Poisson distribution, is used:

$$\eta = e^A \beta^y \quad ; \quad P(y=m) = \frac{c^m e^{-c}}{m!} \quad (19)$$

where A and β are constant parameters, while y is a Poisson distributed random variable with parameter c: $E[y] = c$. The q-order moment of the log-Poisson distribution is thus $\overline{\eta^q} = \exp\left[qA + c\,(\beta^q - 1)\right]$ and the expected scaling of synthetic fields can finally be evaluated:

$$\zeta(q) = 3q + c\,\frac{q\,(\beta - 1) - (\beta^q - 1)}{\ln 2} \quad (20)$$

where the multifractal exponents $\zeta(q)$ depend only on the parameters c and β. In order to display a scaling regime in synthetic fields, parameters c and β must be scale-independent.

Estimates of the model parameters c and β can be obtained by solving the following minimization problem:

$$\min_{c,\beta} \sum_q \left[\frac{\hat{\zeta}(q) - \zeta(q)}{\sigma(q)} \right]^2 \qquad (21)$$

where $\hat{\zeta}(q)$ are the sample multifractal exponents, $\zeta(q)$ is the theoretical expectation (20), and $\sigma(q) = q - 1$ is a weight that accounts for the estimation error, i.e. the standard deviation of $\zeta(q)$. Some sets of numerical simulations were performed with the model presented here with the aim to establish how the standard deviation of $\zeta(q)$ varies with q. Results, not presented here, have shown that $\sigma(q) \sim (q-1)$ holds with a very good approximation independently of parameter values and field resolution.

5 Advection velocity computation and rain sequences selection

The first part of this section is devoted to the estimation of the overall advection velocity of GATE rainfall fields in order to select some sequences for which to perform a self-similar multifractal analysis, assuming temporal anisotropy due only to the storm advection. An investigation of temporal anisotropy induced by self-affinity is also addressed at the end of the section.

The advection velocity U is estimated here using the tracking techniques discussed in detail by Johnson and Bras [1979]. In particular, the centroid method and three composite matching functions are applied with slight modifications to account for the discrete space-time resolution of the GATE dataset. With the centroid technique, storm advection is defined by the movement of the centroid $X(t), Y(t)$, while the other three approaches consist in determining the space shift that maximizes the average cross products or minimizes the square or absolute differences between rainfall fields at different times.

Centroid (C0):

$$X(t) = \frac{\langle x P_{\lambda_x,\lambda_y,\tau}(x,y,t) \rangle}{\langle P_{\lambda_x,\lambda_y,\tau}(x,y,t) \rangle} \qquad Y(t) = \frac{\langle y P_{\lambda_x,\lambda_y,\tau}(x,y,t) \rangle}{\langle P_{\lambda_x,\lambda_y,\tau}(x,y,t) \rangle} \quad (22)$$

Composite matching functions (C1,C2,C3):

$$C1_t(i,j,k) = \left\langle P_{\lambda_x,\lambda_y,\tau}(x,y,t) P_{\lambda_x,\lambda_y,\tau}(x+i\lambda_x, y+j\lambda_y, t+k\tau) \right\rangle \quad (23)$$

$$C2_t(i,j,k) = \left\langle \left[P_{\lambda_x,\lambda_y,\tau}(x,y,t) - P_{\lambda_x,\lambda_y,\tau}(x+i\lambda_x, y+j\lambda_y, t+k\tau) \right]^2 \right\rangle \quad (24)$$

$$C3_t(i,j,k) = \left\langle \left| P_{\lambda_x,\lambda_y,\tau}(x,y,t) - P_{\lambda_x,\lambda_y,\tau}(x+i\lambda_x, y+j\lambda_y, t+k\tau) \right| \right\rangle \quad (25)$$

where $\langle \cdots \rangle$ denotes a spatial average with respect to the x and y axis, $\lambda_x = \lambda_y = 4$ km and $\tau = 15$ minutes are the space and time resolution of the GATE fields, $i\lambda_x$, $j\lambda_y$ and $k\tau$ are thus the spatial shifts and time delay between two matching frames, while $P_{\lambda_x,\lambda_y,\tau}(x,y,t)$ is the integral precipitation (1) on the grid-box at position (x,y) and time t.

The storm velocity components are obtained by $u_x(t) = [X(t+k\tau) - X(t)]/k\tau$ and $u_y(t) = [Y(t+k\tau) - Y(t)]/k\tau$ for the centroid method C0, and by $u_x(t) = \hat{\imath}\lambda_x/k\tau$ and $u_y(t) = \hat{\jmath}\lambda_y/k\tau$ for the other three techniques, where $(\hat{\imath}, \hat{\jmath})$ is the couple of spatial shift indexes that maximizes the composite matching function C1 or that minimizes C2 or C3.

The averages of the storm velocities $U = \langle u(t) \rangle$, where $u(t) = \sqrt{u_x^2(t) + u_y^2(t)}$, were computed for the GATE fields applying the described techniques for delays $k\tau$ from 15 minutes to 2 hours. As shown in Table 1 the estimates of U vary from 12 to 40 km h^{-1}: while the centroid technique estimates the higher velocities for smaller delays, the composite matching functions supply the higher velocities for larger delays. Since these estimates can be influenced by the movements of single cells, while we are interested in the overall advection velocity, the same techniques were also applied to one-hour accumulated fields. In such a way the influence of cell movement is smoothed, since the life-time of convective cells is about 30-40 minutes. The results of this new analysis are presented again in Table 1 for delays of one and two hours and show that the range of mean advection velocity is now reduced to 12-24 km h^{-1}.

Table 1. Mean advection velocities U in km h^{-1} estimated from GATE1 and GATE2 datasets by applying C0, C1, C2 and C3 procedures to 15-minute frames (delays from 15 minutes to 2 hours) and to 1-hour frames (1 and 2 hour delays).

GATE1										
	15-minute frames								1-hour frames	
delays	15'	30'	45'	1h	1h15'	1h30'	1h45'	2h	1h	2h
C0	40.6	31.1	26.8	23.9	21.8	20.2	18.9	17.7	20.5	16.3
C1	14.9	20.4	23.4	24.7	24.5	24.5	24.4	24.6	13.2	20.0
C2	18.5	24.7	26.1	25.8	24.8	24.6	23.6	23.5	13.4	18.9
C3	14.3	18.2	19.3	21.4	21.8	22.2	22.4	22.7	12.1	18.7

GATE2										
	15-minute frames								1-hour frames	
delays	15'	30'	45'	1h	1h15'	1h30'	1h45'	2h	1h	2h
C0	35.8	27.4	23.3	21.0	19.2	17.9	16.7	15.7	18.4	14.6
C1	14.0	17.5	21.1	24.5	25.6	25.8	26.0	25.6	13.7	22.8
C2	15.7	22.1	28.3	29.8	30.0	29.5	28.7	27.2	14.7	23.8
C3	12.9	15.5	19.0	23.9	26.7	27.4	27.3	26.2	12.0	23.2

Due to the discrete resolution in time ($\tau = 15$ min) and space ($\lambda_x = \lambda_y = 4$ km), the GATE datasets allow us to use only some discrete velocities U to perform a space-time multifractal analysis. In the following only the advection velocities $U = 16$ and 32 km h^{-1} are considered, since these values are both compatible with the GATE discretization and with the range of estimates in Table 1.

Let us investigate first if an advection velocity $U = 16$ km h^{-1} can be assumed for a self-similar multifractal analysis in the space-time domain. The larger spatial scale of GATE fields is $L = 64 \times 4$ km $= 256$ km, since each frame is available on a regular grid with 64×64 cells of 4 km on each side. Consequently, the larger time scale must be $T = L/U = 16$ h, while the smaller scales of space and time are the same as the original resolution of GATE fields: $\lambda_0 = 4$ km and $\tau_0 = \lambda_0/U = 15$ minutes.

Several 16-hour rainfall sequences, each comprising 64 consecutive radar scans, were then selected from the original GATE datasets applying the following criteria: i) a moving window in time, collecting 64 consecutive frames, was used to select the strongest rainfall events; ii) each sequence can contain no more that one missing scan; iii) the mean 16-hour rainfall intensity on 256×256 square kilometers I must be larger than 0.25 mm h^{-1}. Some useful information on the 12 and 10 sequences, selected from GATE1 and GATE2 datasets respectively, are summarized in Table 2.

Table 2. The 16-hour sequences selected from GATE1 and GATE2 datasets: F, DAY, and HH are respectively the scan number, the Julian day, and the hour of the first scan of each sequence; I (mm h^{-1}) is the mean 16-hour rainfall intensity on 256×256 square kilometers. Each sequence counts 64 scans.

	GATE1					GATE2			
	F	DAY	HH	I		F	DAY	HH	I
1	832	188	6:15	2.70	1	1156	224	4:13	1.64
2	342	183	1:47	1.52	2	934	221	20:00	1.20
3	1411	194	13:31	1.45	3	1	209	0:00	1.12
4	1485	195	8:01	0.88	4	73	209	18:30	0.74
5	6	179	1:33	0.88	5	776	220	4:15	0.72
6	1549	196	0:14	0.68	6	512	217	6:59	0.67
7	144	180	15:44	0.67	7	1248	225	3:28	0.47
8	406	183	18:02	0.45	8	283	214	21:14	0.35
9	72	179	19:45	0.44	9	209	211	5:15	0.31
10	768	187	14:16	0.41	10	448	216	14:44	0.25
11	224	181	13:45	0.35					
12	566	185	10:30	0.25					

For each 16-hour sequence, the following auto-correlation functions along the x-axis, the y-axis, and the "rescaled" t-axis were compared:

$$
\begin{aligned}
\rho_x(\delta) &= \frac{\langle P_{\lambda_0,\lambda_0,\tau_0}(x,y,t) P_{\lambda_0,\lambda_0,\tau_0}(x+\delta,y,t)\rangle - \mu^2}{\sigma^2} \\
\rho_y(\delta) &= \frac{\langle P_{\lambda_0,\lambda_0,\tau_0}(x,y,t) P_{\lambda_0,\lambda_0,\tau_0}(x,y+\delta,t)\rangle - \mu^2}{\sigma^2} \\
\rho_t(\delta) &= \frac{\langle P_{\lambda_0,\lambda_0,\tau_0}(x,y,t) P_{\lambda_0,\lambda_0,\tau_0}(x,y,t+\delta/U)\rangle - \mu^2}{\sigma^2}
\end{aligned}
\qquad (26)
$$

where $\lambda_0 = 4$ km and $\tau_0 = \lambda_0/U = 15$ minutes, $\langle \cdots \rangle$ is an average in space (x, y) and time (t), μ and σ^2 are the average rainfall and the corresponding variance in each sequence.

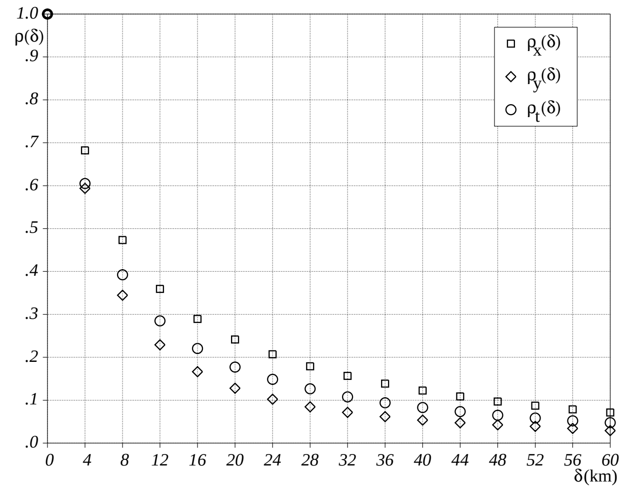

Fig. 4. Mean autocorrelation functions along the x and y directions of the 16-hour sequences selected from the GATE dataset (Table 2) are compared with that along the time axis rescaled with an advection velocity $U = 16$ km h^{-1}.

The average autocorrelation functions obtained from all the selected sequences are plotted in Figure 4. In the Figure, the breakdown of the Taylor hypothesis recognized by Zawadzki [1973] is not evident. For a self-similar process, we expect to find, after having rescaled the time variable with the "correct" storm velocity, the equivalence $\rho_x \equiv \rho_y \equiv \rho_t$ for any δ. This equivalence is not exactly verified by the selected sequences since this analysis has shown that the inequality $\rho_y < \rho_t < \rho_x$ holds for each sequence and for any value of δ, meaning that, in this case, rainfall is more correlated in space along the x-axis than along the y-axis, while the correlation along the rescaled time axis is intermediate.

Despite the fact that the GATE rainfall fields are not exactly isotropic in space, since a preferential direction of motion along the x-axis was always found ($\rho_y < \rho_x$), rainfall fields are often assumed as being isotropic in space, especially for the multifractal analysis and simulation with two-dimensional random cascades. If we accept the isotropy of rainfall fields in space, we can also accept that precipitation is isotropic in the (rescaled)

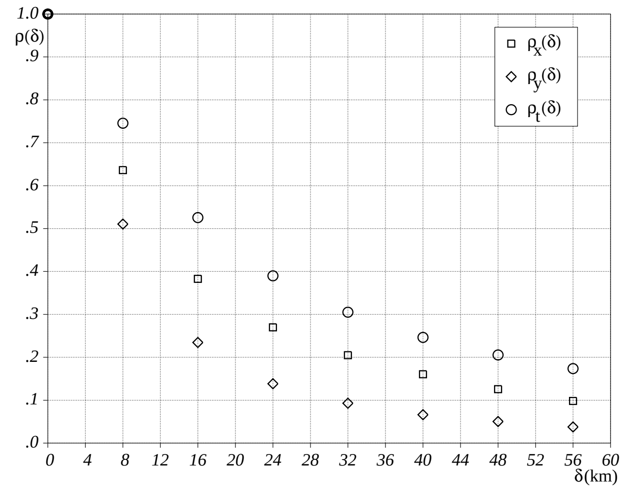

Fig. 5. Mean autocorrelation functions along the x and y directions of the 8-hour sequences selected from the GATE dataset are compared with that along the time axis rescaled with an advection velocity U = 32 km h^{-1}.

space-time domain using the Taylor hypothesis with U = 16 km h^{-1}, since the (rescaled) time axis does not add more anisotropy, as shown by Figure 4.

The hypothesis of a mean advection velocity U = 32 km h^{-1} was also investigated on 8-hour sequences, each composed of 32 radar scans: the higher resolutions are now τ_0 = 15 min and $\lambda_0 = U\tau_0$= 8 km. In this case 21 and 19 sequences were selected from the GATE1 and GATE2 datasets applying the same criteria as above for the 16-hour sequences. From Figure 5, where the average of all the autocorrelation functions are plotted, it is clear that the inequality $\rho_y < \rho_x < \rho_t$ always holds, meaning that the rescaled fields are highly correlated in the time dimension in comparison to the x and y directions, and that a storm velocity U = 32 km h^{-1} cannot be applied for a self-similar multifractal analysis.

Let us now investigate if self-affinity holds for space-time rainfall. This analysis was carried out comparing the one-dimensional temporal power spectra and the one-dimensional spatial power spectra corresponding to each of the selected sequences of Table 2. The estimates of the exponents s_x, s_y, and s_t in (9) together with the estimates $H_x = 1 - s_x/s_t$ and $H_y = 1 - s_y/s_t$ can be found in Table 3. Results show that there exists a great variability in the estimates of H from each sequence and that the estimates H_x are often different from H_y, meaning that self-similarity is not fully verified even in space. The averages of H are always negative and in one case (estimate of H_y from GATE2 sequences) it is zero. To be rigorous, one should consider space-time rainfall as a self-affine process not only with regards to temporal anisotropy but also with regards to the anisotropy due to self-affinity in the $x-y$ plane (since $s_x \neq s_y$). In the sequel of this paper, however, space-time rainfall is simply approximated as a self-similar process (case H = 0) requiring only the determination of the overall advection velocity. This assumption is also suggested by considering that the average of the estimates of H is very small ($\approx$ - 0.12), and that the advantages of the better theoretical accuracy of a self-affine approach would be reduced and perhaps nullified by the uncertainties and large variability in the estimates of both the H and U_0 parameters needed to correctly obtain the scale-dependent velocity U_λ.

Table 3. Estimates of the exponents s_x, s_y, and s_t in (9) and of the scaling anisotropy parameter H from each of the selected sequences of Table 2. The last two rows contain the average μ and standard deviation σ of the estimated parameters.

GATE1						GATE2					
#	s_x	s_y	s_t	H_x	H_y	#	s_x	s_y	s_t	H_x	H_y
1	1.71	1.68	1.34	-0.28	-0.26	1	1.58	1.53	1.36	-0.16	-0.13
2	1.59	1.41	1.30	-0.22	-0.08	2	1.37	1.39	1.12	-0.23	-0.24
3	1.29	1.25	1.07	-0.21	-0.16	3	1.26	1.31	1.10	-0.15	-0.20
4	1.31	1.38	1.00	-0.31	-0.39	4	1.36	1.05	1.17	-0.17	0.10
5	1.46	1.63	1.06	-0.37	-0.54	5	1.31	1.15	1.12	-0.17	-0.02
6	1.26	1.25	1.03	-0.22	-0.21	6	1.39	1.48	1.29	-0.07	-0.15
7	1.40	1.50	1.19	-0.18	-0.26	7	1.21	0.99	1.05	-0.15	0.06
8	1.11	1.14	1.15	0.04	0.01	8	1.53	1.15	1.29	-0.19	0.10
9	1.40	0.89	1.15	-0.22	0.22	9	1.43	1.06	1.37	-0.04	0.23
10	1.62	1.29	1.20	-0.35	-0.08	10	1.13	0.86	1.17	0.03	0.26
11	1.52	1.08	1.09	-0.39	0.00						
12	0.97	0.74	0.90	-0.08	0.17						
μ	1.39	1.27	1.12	**-0.23**	**-0.13**	μ	1.36	1.20	1.20	**-0.13**	**0.00**
σ	0.21	0.28	0.13	0.12	0.22	σ	0.14	0.22	0.12	0.08	0.18

6 Space-time multifractal analysis of GATE rainfall

The space-time multifractal analysis described in section 3.3 is applied here to the 22 selected 16-hour rainfall sequences (Table 2). The analysis is performed assuming rainfall in a self-similar multifractal framework, where the Taylor hypothesis holds with an advection velocity U= 16 km h^{-1}.

Structure functions (6) were computed for each selected precipitation sequence for scales λ ranging from λ_0 = 4 km to L = 256 km, and the corresponding time scales ranging from $\tau_0 = \lambda_0/U$ = 15 minutes to $T = L/U$ = 16 hours. Scaling laws (7) were found to hold with good accuracy for each 16-hour sequence, as is shown in Figures 6 and 7 for the second-order structure functions $S_2(\lambda)$.

The multifractal exponents $\zeta(q)$ of equation (7) were estimated by linear regression of the structure function

Table 4. Results of the multifractal analysis on each sequence of GATE1 dataset: estimates of multifractal exponents $\zeta(q)$; c and β log-Poisson parameters that are solutions of the minimization problem (21); new determination of c_{35} parameters keeping β=0.35 constant; parameters $\tilde{c}$ from (27) used for generation of synthetic space-time rainfall with the STRAIN model.

	$\zeta(q)$					log-Poisson parameters			
	q=2	q=3	q=4	q=5	q=6	β	c	c_{35}	$\tilde{c}$
1	5.52	7.92	10.23	12.48	14.69	0.37	0.81	0.77	0.79
2	5.42	7.64	9.73	11.73	13.67	0.44	1.25	0.99	0.96
3	5.42	7.70	9.88	12.00	14.07	0.34	0.91	0.93	0.98
4	5.39	7.61	9.74	11.80	13.82	0.35	0.98	0.99	1.14
5	5.23	7.26	9.18	11.01	12.78	0.34	1.19	1.23	1.14
6	5.35	7.51	9.55	11.52	13.45	0.38	1.13	1.06	1.22
7	5.24	7.25	9.14	10.95	12.71	0.37	1.30	1.24	1.22
8	5.16	7.01	8.66	10.21	11.72	0.44	1.83	1.44	1.32
9	5.17	7.09	8.90	10.65	12.37	0.34	1.31	1.34	1.32
10	5.06	6.93	8.70	10.43	12.13	0.26	1.17	1.43	1.34
11	5.08	6.96	8.73	10.43	12.09	0.29	1.23	1.42	1.37
12	4.95	6.68	8.31	9.89	11.42	0.26	1.30	1.60	1.43

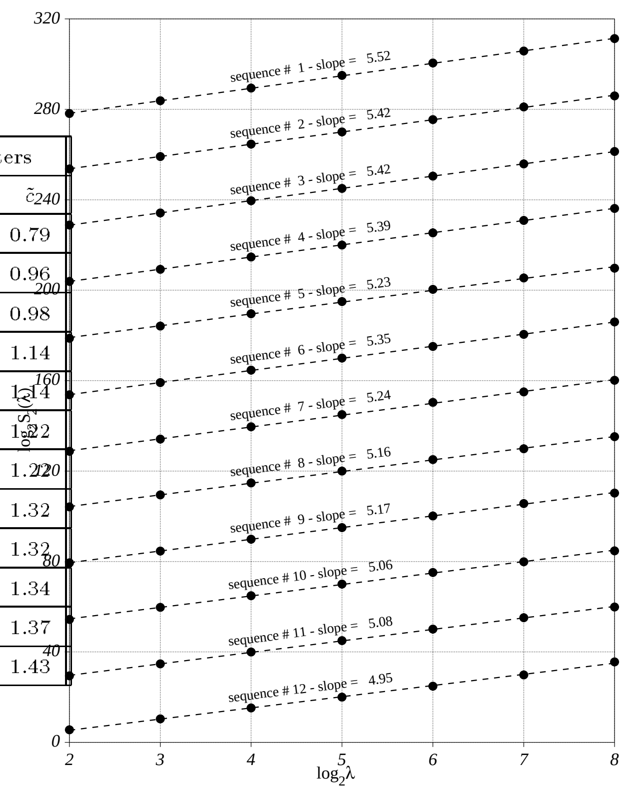

Fig. 6. Log-log plot of the second-order space-time structure functions $S_2(\lambda)$ (equation (6)) of GATE1 sequences versus λ scales ranging from $\lambda_0 = 4$ km to $L = 256$ km (the corresponding time ranges from 15 minutes to 16 hours). Structure functions have arbitrary units to allow displaying of all sequences in the same graph. For each sequence the multifractal exponent $\zeta(2)$, i.e., the slope of the regression line is shown.

$S_q(\lambda)$ versus λ in the log-log plane. They are presented in Tables 4 and 5 for each sequence of GATE1 and GATE2. Sample multifractal exponents (from $q = 2$ to 6) were then used to estimate the two log-Poisson parameters c and β of the STRAIN model by solving the minimization problem (21). As an example, in Figure 8 the sample multifractal exponents estimated for the sequence 5 of GATE1 are plotted together the theoretical expectation (20) having parameters $\beta = 0.34$ and $c = 1.19$ that are solutions of the minimization problem (21). The estimated parameters from all the GATE sequences are presented again in Tables 4 and 5 and are also plotted in Figure 9 versus the averages of the 16-hour rainfall intensity I. While the c parameter decreases as large-scale rainfall rate increases, the β parameter seems to vary around its mean value $\beta = 0.35$ independently of the amount of rainfall.

In order to investigate the dependence of the c parameter on the rainfall intensity, the minimization problem (21) was solved again only for the c parameter, keeping the β parameter constant and equal to the mean value 0.35. These new estimates of the c parameter, called c_{35}, are presented in Tables 4 and 5 and are also plotted in Figure 10, where the dependence of the new estimates c_{35} on the mean intensity I is now more evident than in Figure 9. The following relation was used to express this dependence:

$$\tilde{c} = d \exp(-\gamma I) + c_\infty \qquad (27)$$

When expressing the mean rainfall intensity I in mm h^{-1}, the following parameters, obtained by a best fit procedure applied to the estimates c_{35}, can be used in (27):

Table 5. Same as Table 4, but for GATE2 sequences.

	$\zeta(q)$					log-Poisson parameters			
	q=2	q=3	q=4	q=5	q=6	β	c	c_{35}	$\tilde{c}$
1	5.37	7.57	9.68	11.73	13.74	0.34	0.99	1.01	0.93
2	5.18	7.16	9.03	10.82	12.56	0.32	1.19	1.29	1.04
3	5.33	7.46	9.43	11.27	13.04	0.43	1.40	1.13	1.09
4	5.20	7.20	9.10	10.92	12.70	0.32	1.18	1.26	1.19
5	5.31	7.49	9.58	11.62	13.62	0.28	0.90	1.06	1.20
6	5.32	7.47	9.51	11.48	13.41	0.34	1.07	1.08	1.22
7	5.13	6.99	8.71	10.33	11.92	0.37	1.51	1.43	1.31
8	5.25	7.33	9.32	11.24	13.10	0.30	1.03	1.17	1.37
9	5.14	7.06	8.86	10.60	12.29	0.32	1.28	1.36	1.39
10	5.12	7.02	8.81	10.54	12.22	0.31	1.25	1.38	1.42

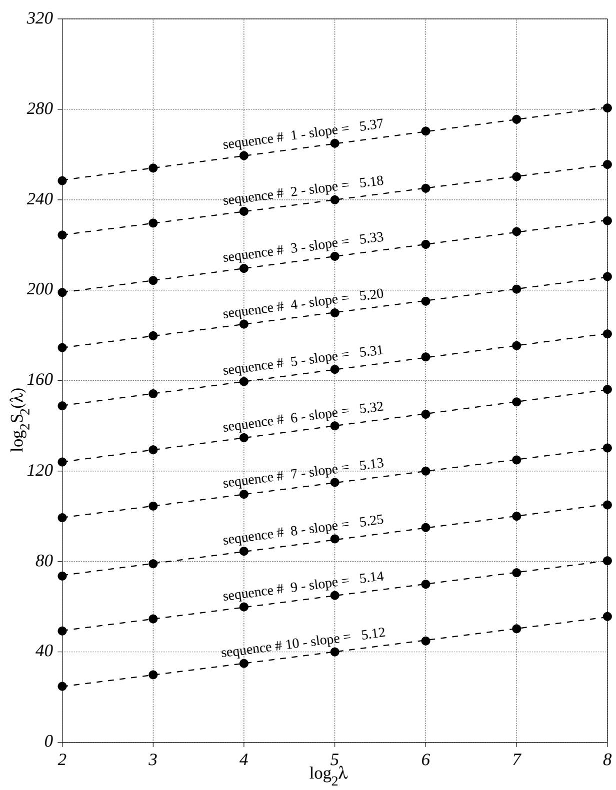

Fig. 7. Same as Figure 6, but for GATE2 sequences.

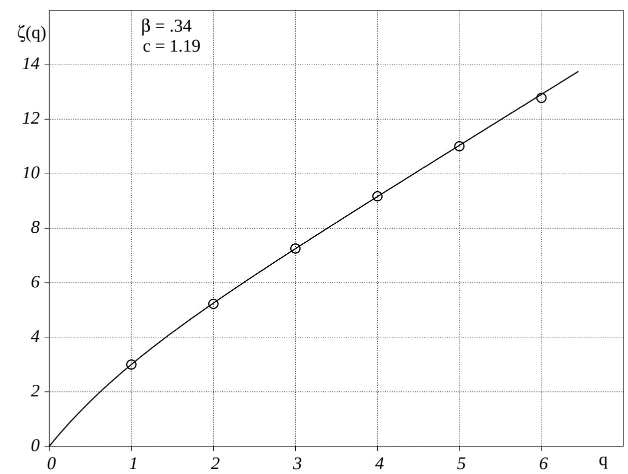

Fig. 8. Sample multifractal exponents estimated for the sequence 5 of GATE1 (circles) are fitted by the theoretical expectation (20) of the STRAIN model (continuous line) having parameters $\beta = 0.34$ and $c = 1.19$ that are solutions of the minimization problem (21).

$a = 0.907$, $\gamma = 0.764$ and the asymptotic value $c_\infty = 0.675$. These values were used to plot (27) in Figure 10 and to determine the c parameters for the simulations of synthetic space-time rainfall presented in next section.

7 Rainfall generation in the space-time domain

The STRAIN model was systematically applied to the generation of space-time rainfall using a constant velocity $U = 16$ km h^{-1} to rescale the time domain. A set of 100 synthetic 16-hour sequences were generated for each of the 22 selected sequences from GATE datasets, providing a total of 2200 realizations. The parameter β was taken constant and equal to 0.35 for all generations, while the values of the c parameter used for each set of 100 generations are reported in the last column of Tables 4 and 5 and are obtained from (27), where the mean rainfall intensity I comes from the corresponding GATE sequence (Table 2). The expansions (11) were truncated at the seventh fragmentation level ($N = 7$) and then reaggregated one level up.

The space-time structure functions (6) and the multifractal exponents $\zeta(q)$ in (7) were estimated on each synthetic field. Figure 11 illustrates that the multifractal behaviour of the observed GATE sequences is well reproducted by synthetic sequences.

A "control" set of 100 simulations were also generated with parameters $\beta = 0.34$ and $c = 1.18$, obtained from (21) when using the averages of the multifractal exponents of the 22 selected sequences (Tables 4 and 5): $\zeta(2) = 5.24$, $\zeta(3) = 7.29$, $\zeta(4) = 9.22$, $\zeta(5) = 11.07$, $\zeta(6) = 12.89$. This control set will be used in the following to investigate how much the statistical properties of space-time rainfall are forced by the large-scale rain rate. Although generated with parameters β and c corresponding to $I = 0.766$ mm h^{-1} in (27), before each comparison the contol set sequences are rescaled to the same amount of rainfall of the comparing GATE sequence. This rescaling does not affect the multifractal behaviour of the control set, but allows quantitative comparisons.

Figure 12 shows the comparisons between the coefficients of variation, skewness, and kurtosis, computed on each of the 22 GATE sequences at the higher resolution (4 km, 15 minutes) and the averages of the corresponding statistics computed on the 22 sets of synthetic rainfall. Figure 12 illustrates that the decreasing trend of the observed statistics as the average rain intensity I increases is reproduced by the sets of synthetic fields. It is also apparent that taking the same model parameters for different large-scale rain rates, as in the control set (whose statistics are also reported in Figure 12 with dashed lines), we cannot reproduce this feature.

The cumulative distribution functions (CDFs) of rainfall intensity i at the higher resolution (again 4 km, 15 minutes) were also computed from each GATE sequence and compared with the 90% confidence limits obtained by the corresponding sets of synthetic rainfall. Figures 13 and 14 show that in most of the cases the observed CFDs are within the 90% confidence limits and that the STRAIN model is able to correctly reproduce also the most rare and intense rain rates. From Figures 13 and 14 it is also apparent that sometimes the highlighted dependence of the c parameter on the large-scale rainfall rate I, as expressed by (27), is not able to completely explain the variability of the statistics of the observed rainfall, meaning that a better determination of model parameters based also on the type of precipitation event could be necessary. For instance, if we consider sequences 4 and 5 from GATE1 we can observe that, although in both sequences the large-scale rainfall rate is $I = 0.88$ mm h^{-1}, so that (27) gives $\tilde{c} = 1.14$, in the first case the right-hand tail of the CDF is over-estimated by synthetic rainfall, while in the second case it is under-estimated. Similar considerations can be made also for other sequences, for instance number 6 and 7 from GATE1 have respectively $I = 0.67$ and I=0.68, giving $\tilde{c} = 1.22$ from (27); while the CDF of sequence 6 exceeds of the 90% confidence limits, the CDF of sequence 7 is well-reproduced by synthetic rainfall.

In Figure 15 the CDF of the first sequence from GATE1 is compared with the 90% confidence limits obtained by the control set of synthetic rainfall. Analyzing the right-hand tail of the CDF in Figure 15 it is apparent that the most intense rain rates in the control set are about three times bigger than those in the observed sequence. The comparison with Figure 13 points out again the need to downscale rainfall using model parameters that change at least with the large-scale rain rate, as in (27).

The last comparison between observed and synthetic space-time rainfall addresses the feature of the areal reduction factors (ARFs). There are several definitions of ARFs; the most widely applied are: i) the ratio between average rainfall depth over an area, for example a catchment, and the maximum rainfall depth measured in a point within the considered area, for example by a rain-gage (fixed-area ARFs); and ii) the ratio of average storm depth over an area, delimited for instance by rainfall isohyets, and the maximum rainfall depth at the storm center (storm-centered ARFs). The comparisons discussed here regard fixed-area ARFs, but, since point rainfall is not available for GATE fields, we considered instead the rainfall depth at the higher spatial resolution (4 km $\times$ 4 km).

Let $h_{\lambda,\lambda,\tau} = P_{\lambda,\lambda,\tau}/\lambda^2$ be the average rainfall depth over an area $\lambda \times \lambda$ accumulated over a time τ. ARFs are computed from both observed and synthetic sequences as $\alpha(\lambda) = h_{\lambda,\lambda,\tau}/\hat{h}_{\lambda_0,\lambda_0,\tau}$, where $\hat{h}_{\lambda_0,\lambda_0,\tau}$ is the maximum rainfall depth in the fixed accumulation time τ over an area $\lambda_0 \times \lambda_0$ (in our case $\lambda_0 = 4$ km) embedded in $\lambda \times \lambda$. Figure 16, where the average ARFs of the 22 observed GATE sequences are shown to be very close to those obtained by the 2200 synthetic ones, illustrate how the STRAIN model is also able to reproduce the observed ARFs for different accumulation times τ.

8 Summarizing conclusions

The development of a space-time rainfall downscaling procedure is crucial in coupling meteorological to hydrological models, since we have to fill the gap between the large scales of space and time over which meteorological models supply rainfall predictions and the natural scales of basins' response as required by hydrological rainfall-runoff modeling. The STRAIN model is suggested here as a useful tool for simulation of space-time rainfall displaying self-similarity, scale covariance and the same multifractal behavior as the observed precipitation. The model can be tuned by three parameters: the overall advection velocity U, and the log-Poisson parameters c and β.

It was pointed out how the multifractal behaviour of rainfall depth in space depends on the accumulation time, and, similarly, how the set of multifractal exponents that characterize the anomalous scaling of rainfall in time depends on the spatial extension. A direct space-time rainfall downscaling enables determination of sets of multifractal exponents not dependent on the spatial extension and on the accumulation time.

In principle, the downscaling problem can be addressed in a multifractal framework by assuming space-time rainfall to be a self-similar or a self-affine process. Following the former approach one only has to determine the overall advection velocity of the storm, while the self-affine multifractal modeling requires estimation of the scaling anisotropy parameter H as well. In GATE datasets, this last parameter was found to be negative on average, but not very different from zero, meaning that space-time rainfall can be approximated by a self-similar multifractal process. The simpler self-similar approach, followed in this paper, is also suggested by the great variability and uncertainty in estimating both the advection velocity and the parameter H.

A space-time multifractal analysis of selected GATE sequences has revealed that a very good scaling of structure functions holds from 4 to 256 km in space, and from 15 minutes to 16 hours. A dependence of the multifractal behavior of space-time rainfall on the large-scale rain rate was then highlighted and a very simple equation relating the c parameter to the average rainfall intensity I at the larger scales of space and time was proposed.

The STRAIN model was systematically applied to downscale the GATE selected sequences, keeping constant the advection velocity $U = 16$ km h^{-1} and the parameter $\beta = 0.35$, and varying the c parameter according to the average rainfall intensity I observed in each GATE sequence. The comparisons between observed and synthetic rainfall presented in this paper, in terms of multifractal behaviour, of moments of rainfall at the lower scales, of cumulative distribution functions, and areal reduction factors, have shown that the STRAIN model is able to correctly reproduce many of the statistical properties observed in GATE rainfall and their dependence on the large-scale rain rate. It was also pointed out that space-time rainfall sequences characterized by different average rainfall intensities cannot be downscaled using the same model parameters, and that a better explanation of the variability in the observed statistics could be pursued by refining the dependence of the model's parameters not only on the large-scale rain rate, but also on the type of precipitation event.

Acknowledgements. The research was supported by the Sardinia Regional Authorities. The author thanks Prof. Franco Siccardi and Prof. Roberto Benzi for the stimulating discussions on the topics of this paper, and two anonymous reviewers for their in-depth suggestions for improving the manuscript.

References

Benzi, R., Paladin, G., Parisi, G., and Vulpiani, A., On the multifractal nature of fully developed turbulence and chaotic systems, *J. Phys. A*, *17*, 3521–3531, 1984.

Deidda, R., Multifractal analysis and simulation of rainfall fields in space, *Phys. Chem. Earth (B)*, *24*(1-2), 73–78, 1999.

Deidda, R., Benzi, R., and Siccardi, F., Multifractal modeling of anomalous scaling laws in rainfall, *Water Resour. Res.*, *35*(6), 1853–1867, 1999.

Dubrulle, B., Intermittency in fully developed turbulence: log-Poisson statistics and generalized scale-covariance, *Phys. Rev. Lett.*, *73*, 959–962, 1994.

Fabry, F., On the determination of scale ranges for precipitation fields, *J. Geophys. Res.(D)*, *101*(D8), 12819–12826, 1996.

Falconer, K. J., *Fractal Geometry: Mathematical Foundations and Applications*, John Wiley and Sons, Inc., Chichester, 1990.

Feder, J., *Fractals*, Plenum Press, New York, 1988.

Georgakakos, K. P., Carsteanu, A. A., Sturdevant, P. L., and Cramer, J. A., Observation and analysis of midwestern rain rates, *J. Appl. Meteor.*, *33*, 1433–1444, 1994.

Gupta, V. K. and Waymire, E. C., A statistical analysis of mesoscale rainfall as a random cascade., *J. Appl. Meteor.*, *32*, 251–267, 1993.

Hubert, P., Tessier, Y., Lovejoy, S., Schertzer, D., Schmitt, F., Ladoy, P., Carbonnel, J. P., Violette, S., and Desurosne, I., Multifractals and extreme rainfall events., *Geophys. Res. Lett.*, *20*(10), 931–934, 1993.

Hudlow, M. D. and Patterson, V. L., GATE Radar Rainfall Atlas, NOAA Special Report, U.S. Dept. of Commer., Washington, D.C., 1979.

Johnson, E. R. and Bras, R. L., Real-time estimation of velocity and covariance structure of rainfall events using telemetered raingauge data: a comparison of methods, *J. Hydrol.*, *44*, 97–123, 1979.

Kumar, P. and Foufoula-Georgiou, E., A multicomponent decomposition of spatial rainfall fields. Part 1: Segregation of large- and small-scale feature using wavelet tranform., *Water Resour. Res.*, *29*(8), 2515–2532, 1993.

Kumar, P. and Foufoula-Georgiou, E., A multicomponent decomposition of spatial rainfall fields. Part 2: Self-similarity in fluctuations., *Water Resour. Res.*, *29*(8), 2533–2544, 1993.

Ladoy, P., Schmitt, F., Schertzer, D., and Lovejoy, S., Variabilité multifractale des observations pluviométriques à Nîmes, *C. R. Acad. Sci. Paris*, *317, Série II*, 775–782, 1993.

Lebel, T., Braud, I., and Creutin, J.-D., A space-time disaggregation model adapted to Sahelian mesoscale convective complexes, *Water Resour. Res.*, *34*(7), 1711–1726, 1998.

Lovejoy, S. and Schertzer, D., Generalized scale invariance and fractal models of rain, *Water Resour. Res.*, *21*, 1233–1250, 1985.

Lovejoy, S. and Schertzer, D., Multifractals, universality classes, and satellite and radar measurements of cloud and rain fields, *J. Geophys. Res.*, *95*, 2021–2031, 1990.

Marsan, D., Schertzer, D., and Lovejoy, S., Casual space-time multifractal processes: predictability and forecasting of rain fields, *J. Geophys. Res.(D)*, *101*(D21), 26333–26346, 1996.

Menabde, M., Harris, D., Seed, A., Austin, G., and Stow, D., Multiscaling properties of rainfall and bounded random cascades, *Water Resour. Res.*, *33*(12), 2823–2830, 1997.

Monin, A. S. and Yaglom, A. M., *Statistical Fluid Mechanics*, vol. 1, MIT Press, Cambridge, Mass, 1971.

Monin, A. S. and Yaglom, A. M., *Statistical Fluid Mechanics*, vol. 2, MIT Press, Cambridge, Mass, 1975.

Olson, J. and Niemczynowicz, J., Multifractal analysis of daily spatial rainfall distributions, *J. Hydrol.*, *187*, 29–43, 1996.

Over, T. M. and Gupta, V. K., Statistical analysis of mesoscale rainfall: dependence of a random cascade generator on large-scale forcing., *J. Appl. Meteor.*, *33*, 1526–1542, 1994.

Rodriguez-Iturbe, I., Febres de Power, B., Sharifi, M. B., and Georgakakos, K. P., Chaos in rainfall, *Water Resour. Res.*, *25*(7), 1667–1675, 1989.

Schertzer, D. and Lovejoy, S., Generalized scale invariance in turbulent phenomena, *Phys. Chem. Hydrodyn.*, *6*, 623–635, 1985.

She, Z.-S. and Leveque, E., Universal scaling laws in fully developed turbulence, *Phys. Rev. Lett.*, *72*, 336–339, 1994.

She, Z.-S. and Waymire, E. C., Quantized energy cascade and log-Poisson statistics in fully developed turbulence, *Phys. Rev. Lett.*, *74*, 262–265, 1995.

Svensson, C., Olson, J., and Berndtsson, R., Multifractal properties of daily rainfall in two different climates, *Water Resour. Res.*, *32*(8), 2463–2472, 1996.

Taylor, G. I., The spectrum of turbulence, *Proc. Roy. Soc. Lon.*, *A164*(919), 476–490, 1938.

Tessier, Y., Lovejoy, S., and Schertzer, D., Universal multifractals: theory and observations for rain and clouds, *J. Appl. Meteor.*, *32*(2), 223–250, 1993.

Yaglom, A. M., Effect of fluctuations in energy dissipation rate on the form of turbulence characteristics in the inertial subrange, *Dokl. Akad. Nauk SSSR*, *166*, 49–52, 1966.

Zawadzki, I. I., Statistical properties of precipitation patterns, *J. Appl. Meteor.*, *12*, 459–472, 1973.

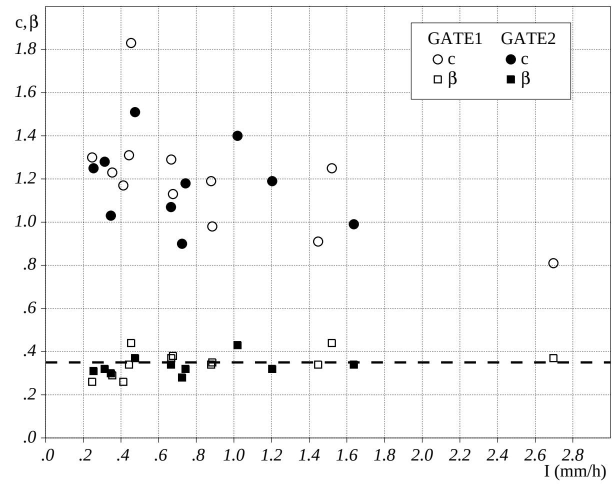

Fig. 9. Plot of log-Poisson coefficients c (circles) and β (squares), solutions of the minimization problem (21), versus the 16-hour rainfall intensity I over 256×256 square kilometers for the GATE1 (empty symbols) and GATE2 (filled symbols) sequences. The dashed line is drawn for the mean value $\beta = 0.35$.

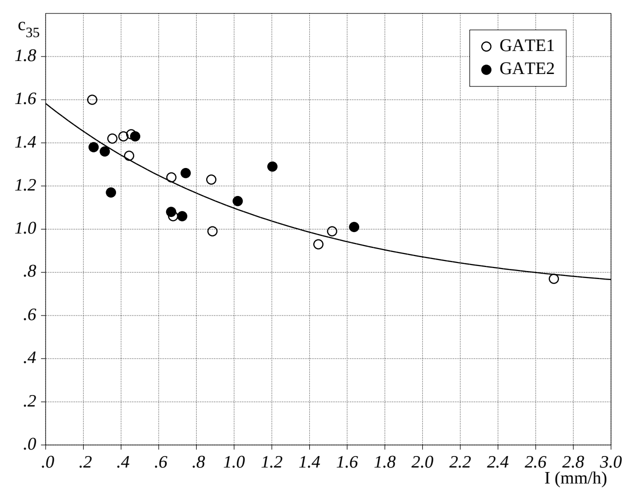

Fig. 10. Plot of log-Poisson coefficients c_{35}, solution of the minimization (21) keeping β=0.35 constant, versus the 16-hour rainfall intensity I over 256×256 square kilometers for the GATE1 (empty circles) and GATE2 (filled circles) sequences. Continuous line represents a best fit regression and is plotted using equation (27).

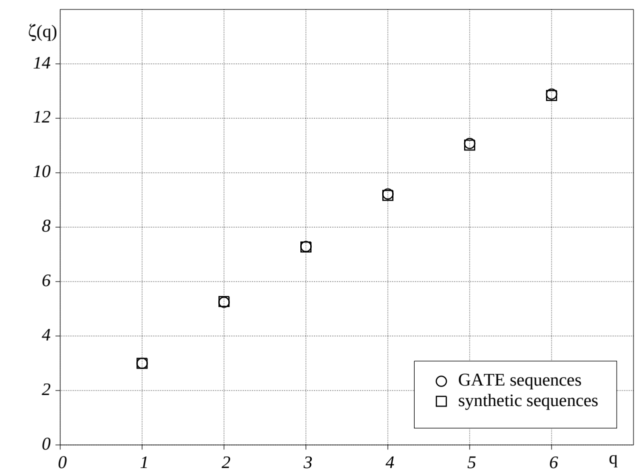

Fig. 11. Averages of multifractal exponents of the original GATE sequences (circles) are compared with those estimated from the synthetic sequences (squares).

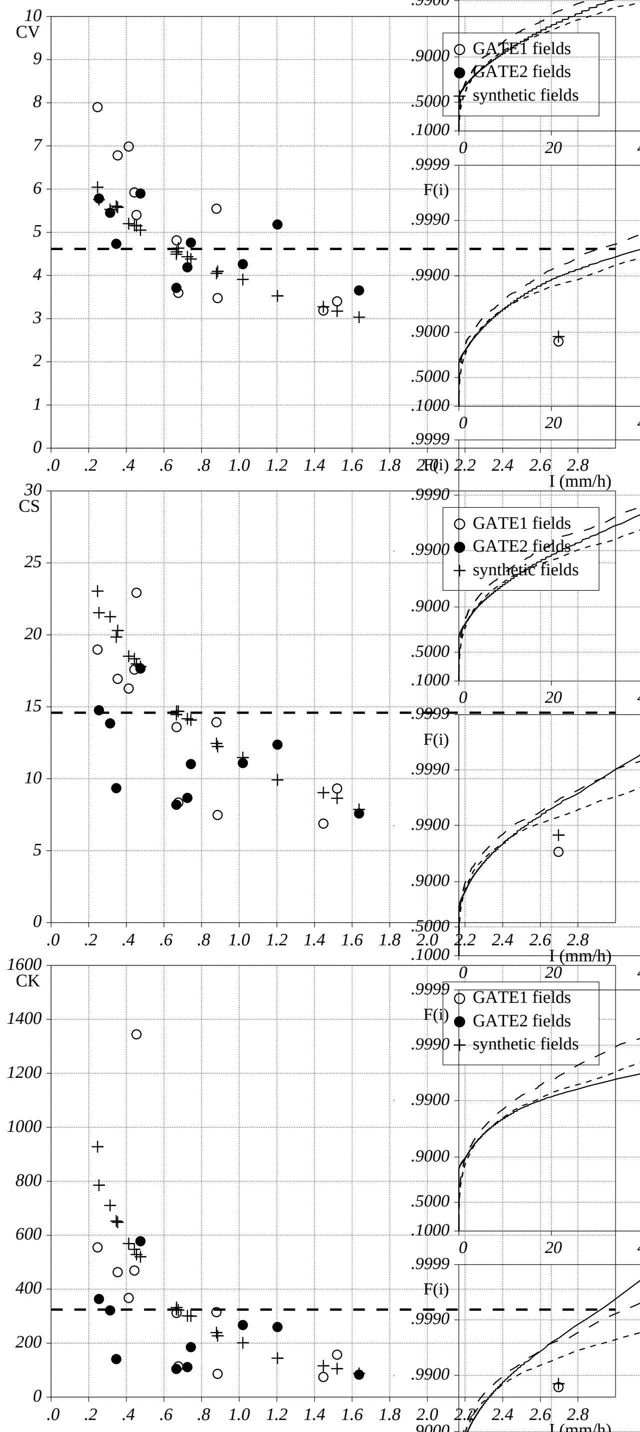

Fig. 12. Comparisons between the coefficients of variation CV (top), the coefficient of skewness CS (middle), and coefficient of kurtosis CK (bottom) estimated from the GATE sequences (circles) and from the synthetic ones (crosses), generated with parameters $\beta = 0.35$ and c from Eq. (27). The dashed lines mark the statistics of the "control" set of synthetic fields generated with constant parameters $\beta = 0.34$ and $c = 1.18$.

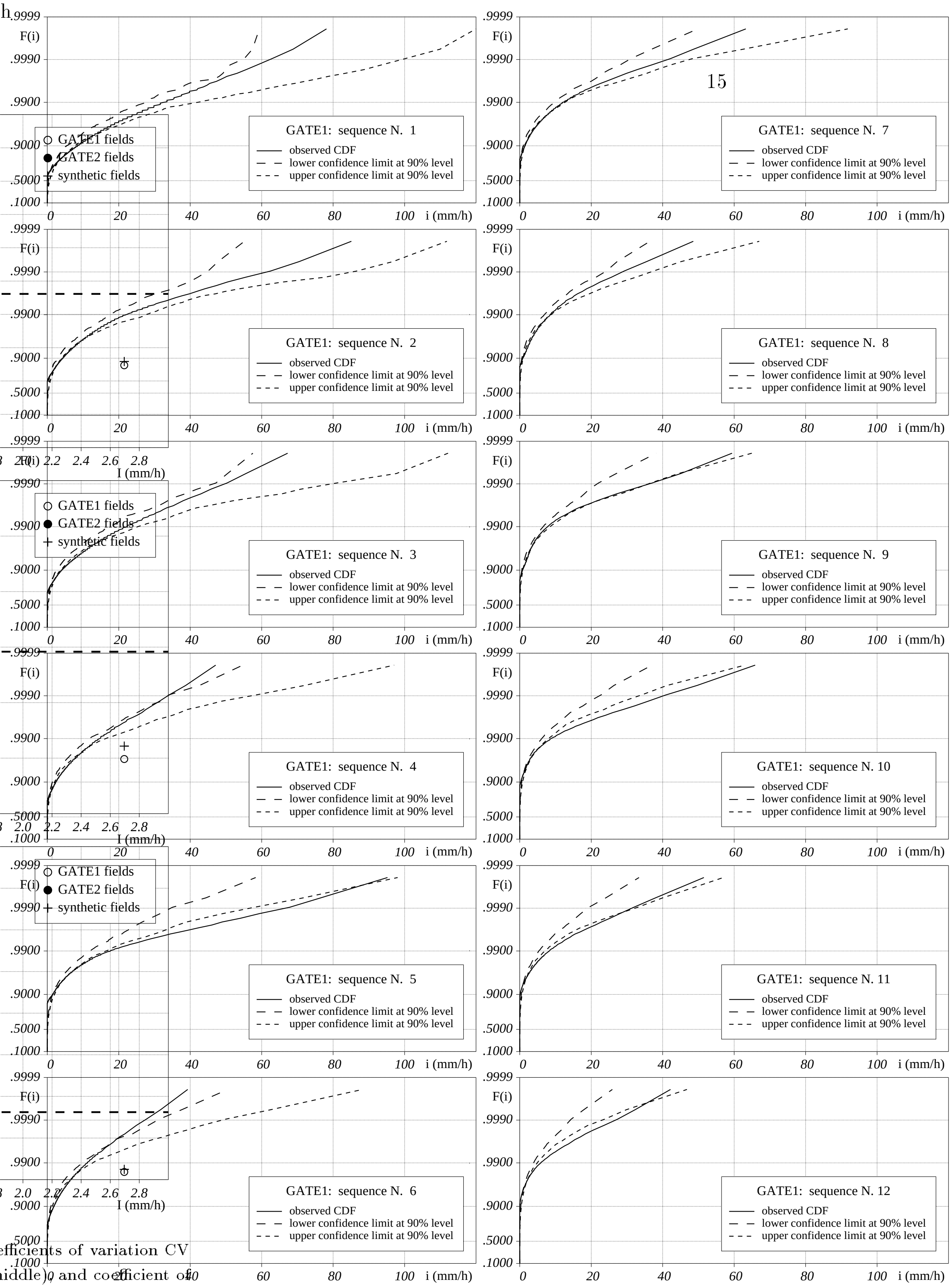

Fig. 13. Cumulative distribution functions $F(i)$ of rainfall rate i (mm h^{-1}) at higher resolution (4 km $\times$ 4 km, 15 minutes) obtained from each GATE1 sequence are compared with the 90% confidence limits estimated from synthetic fields, generated with parameter $\beta = 0.35$ and c from equation (27). Points of CDFs are averages over 100 sorted rain rates.

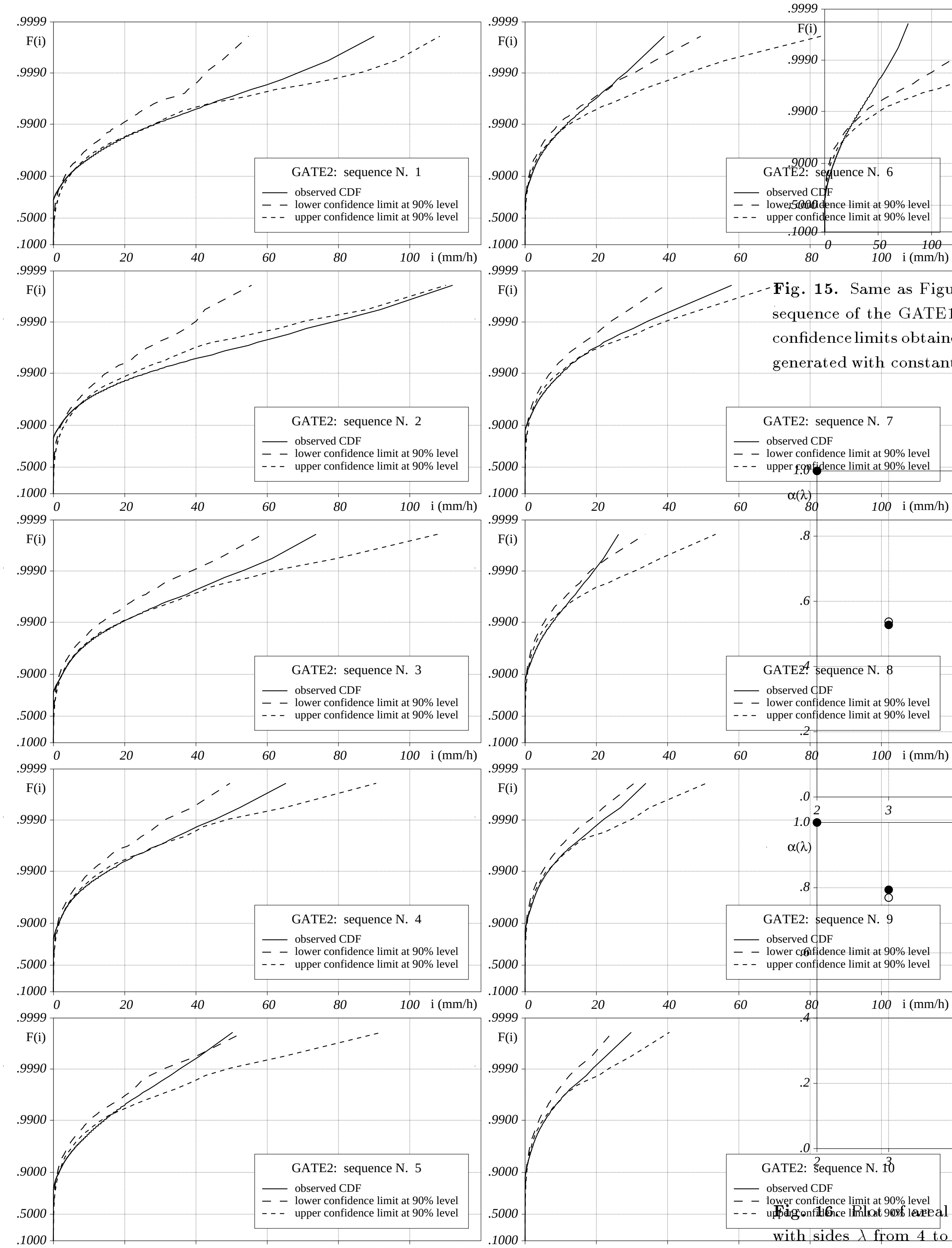

Fig. 14. Same as Figure 13, but for GATE2 sequences.

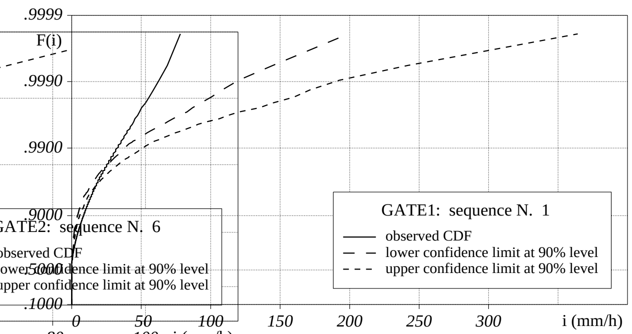

Fig. 15. Same as Figure 13, but the CDF observed in the first sequence of the GATE1 dataset is now compared with the 90% confidence limits obtained by the "control" set of synthetic rainfall generated with constant parameter $\beta = 0.34$ and $c = 1.18$.

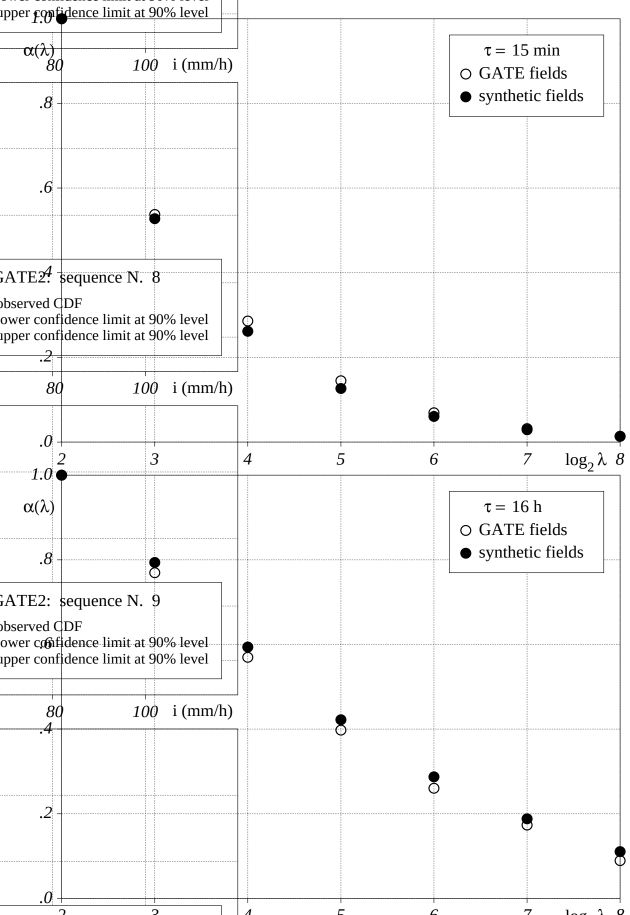

Fig. 16. Plot of areal reduction factors $\alpha(\lambda)$ over square areas with sides λ from 4 to 256 km. ARFs for rainfall depths accumulated over 15 minutes (left) and 16 hours (right) computed for GATE fields (empty circles) are compared with those obtained from synthetic sequences (filled circles).